JTTEE5 16:722–728
DOI: 10.1007/s11666-007-9103-y
1059-9630/$19.00 © ASM International

PEER REVIEWED

Molecular Dynamics Simulation of Flattening Process of a High-Temperature, High-Speed Droplet—Influence of Impact Parameters

J. Shimizu, E. Ohmura, Y. Kobayashi, S. Kiyoshima, and H. Eda

(Submitted March 10, 2007; in revised form June 5, 2007)

Three-dimensional molecular dynamics simulation was conducted to clarify at an atomic level the flattening process of a high-temperature droplet impacting a substrate at high speed. The droplet and the substrate were assumed to consist of pure aluminum, and the Morse potential was postulated between a pair of aluminum atoms. In this report, the influence of the impact parameters such as the droplet velocity and the droplet diameter on flattening behavior were analyzed. As a result, the following representative conclusions were obtained: (a) the flattening ratio increases in proportion to the droplet velocity and the droplet diameter; (b) the flattening ratio for nanosized droplet can be reorganized by the same dimensionless parameters of the proper physical properties, such as the viscosity and the surface tension, as those used in the macroscopic flattening process.

Keywords droplet, flattening, impact parameter, molecular dynamics, solidification

1. Introduction

Deposition with high-temperature, high-speed droplets such as by thermal spraying is widely used (Ref 1). In particular, it is often applied to the coating of functional materials that are difficult to machine because a comparatively thick coating (i.e., from a few tens to a few hundreds micrometers) can be obtained in a relatively short time.

On the other hand, the pulsed laser deposition (PLD) technique is employed to form fine thin films (i.e., a few tens of Angstroms to a few nanometers) using high-temperature, high-speed droplets with a diameter of nanometer or hundred-nanometer order (Ref 2, 3). In this case, the use of finer droplets and denser organization of the thin film increases the strength of the thin film, making it advantageous for application to ultraprecise electronic, magnetic, or optical devices.

It is important to understand the flattening behavior of a droplet as the elementary process involved in order to clarify the adhesion state, residual stress, and the other physical properties. Many researchers have studied the flattening behavior of droplets (Ref 4-18). Some mechanical models with different assumptions have been proposed, and thermohydrodynamic calculations and experiments have been reported for a limited range of materials and conditions. However, the results do not always agree with each other, and a theory that can satisfactorily estimate the flattening behavior of a droplet has not yet been fully developed. One reason for this is the difficulty of theoretically analyzing the impact and flattening processes of a droplet, since its change of shape is so drastic. It is also difficult to experimentally verify the behavior of a droplet, because the processes take place in a time span of microseconds for a small droplet of micrometer order.

Rather than conducting conventional continuum modeling, we considered an atomistic model that can flexibly deal with drastic physical change using the molecular dynamics method. The molecular dynamics simulation can handle the materials phase transformation as well as nanoscopic phenomena. Therefore, there have been many applications, such as the formation process of a carbon nanotube by chemical vapor deposition (Ref 19), the lubrication process of the lubricant (Ref 20), the nanomachining process of the silicon wafer (Ref 21), and so on. However, the atomistic model also has some limitations, such as the number of atoms that can be treated, and the interatomic potential between different atoms has not always been clarified. Nevertheless, we tried to elucidate the targeted phenomenon using an atomistic model because such an approach has not yet been made and presents a high potential.

This article is an invited paper selected from presentations at the 2007 International Thermal Spray Conference and has been expanded from the original presentation. It is simultaneously published in *Global Coating Solutions, Proceedings of the 2007 International Thermal Spray Conference*, Beijing, China, May 14-16, 2007, Basil R. Marple, Margaret M. Hyland, Yuk-Chiu Lau, Chang-Jiu Li, Rogerio S. Lima, and Ghislain Montavon, Ed., ASM International, Materials Park, OH, 2007.

J. Shimizu and **H. Eda**, Department of Intelligent Systems Engineering, Ibaraki University, Hitachi, Ibaraki, Japan; **E. Ohmura**, Graduate School, Osaka University, Suita, Osaka, Japan; **Y. Kobayashi**, Tocalo Co., Ltd., Akashi, Hyogo, Japan; and **S. Kiyoshima**, Research Center of Computational Mechanics, Inc., Shinagawa, Tokyo, Japan. Contact e-mail: jshimizu@mx.ibaraki.ac.jp.

As the first step, we conducted molecular dynamics analysis of the impact of a globular high-temperature, high-speed aluminum (Al) droplet on a flat Al substrate (Ref 22). We investigated the flattening process and clarified the processes of melting and solidification, temperature distribution, deformation velocity, and potential energy of atoms of the droplet. In this paper, the influences of the impact parameters, such as droplet velocity and droplet diameter, on its flattening behavior are analyzed, and the flattening ratio is described by dimensionless numbers.

1.1 Molecular Dynamics Simulation Model

The proposed model for three-dimensional molecular dynamics analysis is shown in Fig. 1. The substrate surface is Al(001) and is assumed to have a perfectly smooth surface at the atomic level. By considering the mass of atom i to be m, its position vector at the time step t to be $\mathbf{r}_i(t)$, and the resultant force vector of all forces acting from other atoms to be $\mathbf{F}_i(t)$, the following equation of motion is obtained:

$$m\frac{d^2\mathbf{r}_i(t)}{dt^2} = \mathbf{F}_i(t) \quad \text{(Eq 1)}$$

$\mathbf{F}_i(t)$ is calculated using:

$$\mathbf{F}_i(t) = -\sum_{j\neq i} \text{grad } \phi_{ij} \quad \text{(Eq 2)}$$

where ϕ is the interatomic potential depending on the distance between atoms, and the index j indicates atoms others than atom i. The numerical integration of Eq 1 is carried out using the leapfrog method (Ref 23) with a time step of 3 fs.

The following Morse potential, which requires a comparatively short calculation time, is applied as the interatomic potential to handle as many atoms as possible:

$$\phi(r) = D[\exp\{-2\alpha(r-r_0)\} - 2\exp\{-\alpha(r-r_0)\}] \quad \text{(Eq 3)}$$

where r is the atomic distance between a pair of atoms, D is the dissociation energy, α is the potential coefficient, and r_0 is the equilibration distance. Here, the parameters for aluminum described in Ref 24 are applied as: $D = 0.2703$ eV, $\alpha = 1.1646$ Å^{-1}, $r_0 = 3.253$ Å.

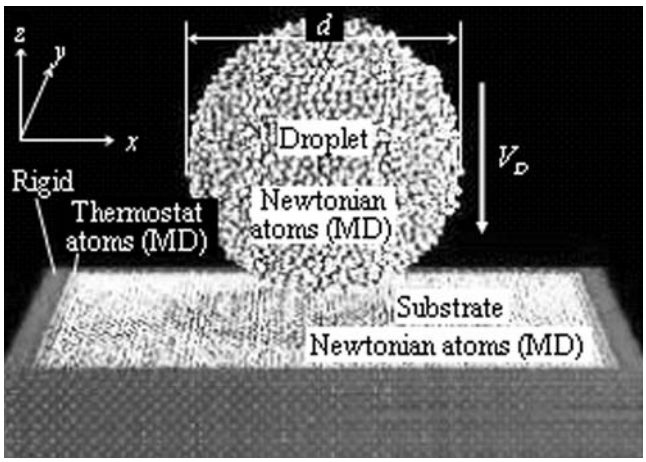

Fig. 1 Molecular dynamics simulation model

The dimensions of the substrate analysis area in the x, y, and z directions are $100a \times 100a \times 5a$, respectively, where, a is the lattice constant of aluminum and equals 0.4 nm. The uppermost part of the analysis area of the substrate is assumed to be a free surface. Outside the analysis area except for the free surface, atoms are arrayed in a lattice of constant length as the temperature control layer. Energy can dissipate from this layer when mechanical energy is generated inside the analysis area. The area outside the temperature control layer is assumed to be a perfect rigid body. The simulations were performed in a perfect vacuum without considering the ambient air or gas to purely examine the effect of droplet speed and size in the splat formation process. Here, the axisymmetric model was not used to prevent the generation of extra dislocation in the boundary, although the number of atoms to handle is limited.

Considering the principle of minimum potential energy, atomic arrays of Al were obtained at absolute zero temperature, then atomic arrays at 1500 and 300 K for the droplet and substrate, respectively, were arranged considering thermal expansion, and mean-velocity vectors at corresponding temperatures were randomly assigned to all atoms. Next, Newton's motion equations were solved and velocity scaling was implemented sequentially until the system became stable. As a result, an atomic array model with a surface was constructed. It was also confirmed that the velocity of the atoms followed Maxwell distributions (Ref 25). These results confirmed the validity of the initial array models constructed, respectively, for the substrate and the droplet.

All the simulations were calculated using a self-made code written in Fortran77 and operated on computers equipped with Pentium IV 3 GHz CPU and 1 GB memory. The calculation time for a simulation in a period of 60 ps (20,000 steps) was about 200 h, average duration.

2. Simulation Results and Discussions

The parameters of the molecular dynamics simulation discussed in this paper are listed in Table 1. The influences of the impact parameters, such as droplet velocity and droplet diameter, on its flattening behavior and flattening ratio were analyzed. The flattening ratio is defined as $\xi = D/d$, where D is the maximum diameter of the droplet during or after flattening. Then the impact and deformation processes of a droplet with a temperature of 1500 K (which is about 550 K higher than the melting point of aluminum), diameters of $d = 3.1$ to 12.4 nm, and velocities of $V_D = 500$ to 2500 m/s were considered. A very large range of velocities are necessary to analyze the sufficient splat formation as observed in the practical thermal spray processes, because the inertia of the droplet is extremely small in the case of nanosized droplet flattening.

2.1 Influence of Droplet Velocity

The influence of the droplet velocity on the flattening behavior is discussed here using a droplet with a diameter of 12.4 nm. The parallel-to-substrate traveling distance and the behavior of the atoms in the droplet and substrate are shown in Fig. 2 for V_D in the range of 500 to 2500 m/s. The gray scale displays the horizontal traveling distance of the droplet atom. The time when the droplet contacts the substrate surface is set at $t = 0$. The snapshots in Fig. 2 display the cross section at the center line of the droplet.

Table 1 Simulation parameters

Droplet	Aluminum (Al)
Substrate	Aluminum (Al, $a = 0.4$ nm)
Analyzed area of substrate	$100a \times 100a \times 5a$ (40 nm × 40 nm × 2 nm)
Inter-atomic potential	Morse
Initial temperature, K	
Droplet temperature (T_d)	1500
Substrate temperature (T_s)	300
Droplet diameter (d), nm	3.1-12.4
Droplet velocity (V_D), m/s	500-2500

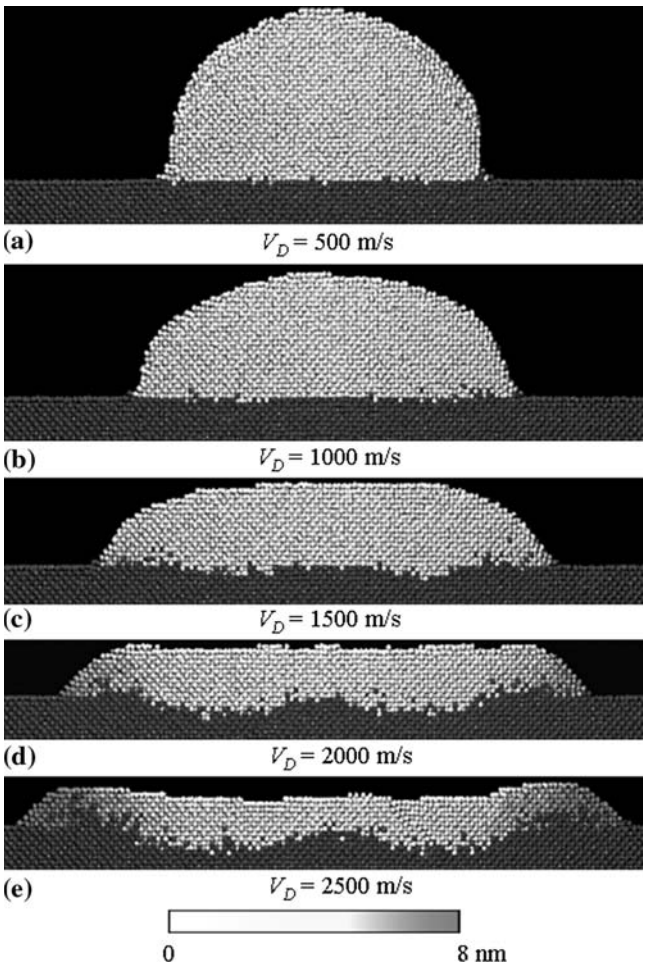

Fig. 2 Deformation process of droplet and traveling distance of atoms in horizontal direction ($d = 12.4$ nm). V_D = (a) 500 m/s, (b) 1000 m/s, (c) 1500 m/s, (d) 2000 m/s, and (e) 2500 m/s

From this figure, it can be understood that the deformation in the parallel-to-substrate direction becomes larger in proportion to the droplet velocity.

To clarify the transfer or flow of the atoms in the droplet, the atomic trajectories in representative positions in the droplet are shown in Fig. 3 for $V_D = 500$, 1500, and

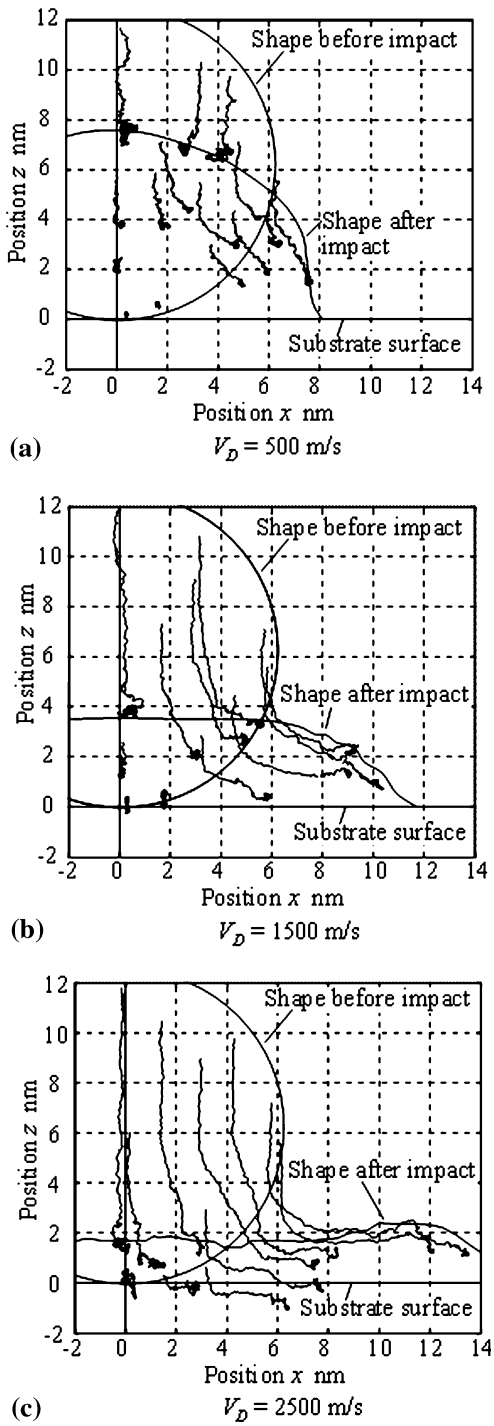

Fig. 3 Trajectory of some atoms in droplet ($d = 12.4$ nm). V_D = (a) 500 m/s, (b) 1500 m/s, and (c) 2500 m/s

2500 m/s, respectively. These results demonstrate that the transfer of atoms in the droplet to the parallel-to-substrate direction increases in proportion to the horizontal distance from the central axis of the droplet, independent of droplet velocity.

The instantaneous potential energy of each atom is examined next to clarify the relationship between the droplet velocity and the resolidification process. Figure 4 shows the potential energy of each atom in the resolidification process for $V_D = 500$, 1500, and 2500 m/s, respectively. The potential energy corresponds to the strain energy and increases in a position where the perfect crystallinity is disturbed by generation of defects, such as the dislocations or in the vicinity of the surface. The potential energy is assumed to be zero when the inside of the material is in thermal equilibrium at 300 K. In Fig. 4, the regions are divided by a solid line according to the arrangement and potential energy of the atoms, so that it can be roughly understood whether or not recrystallization has yet occurred. Here, the right side of the droplet from the center axis has been enlarged to clearly observe the crystal arrays, on the assumption that the deformation process occurs axisymmetrically.

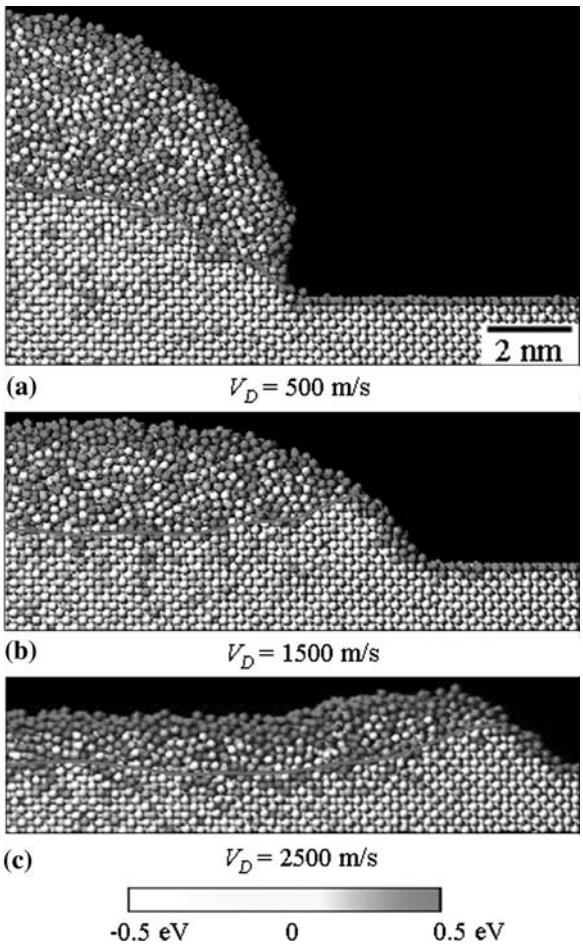

Fig. 4 Relationship between deformation and solidification process of droplet and potential energy of atoms ($d = 12.4$ nm). V_D = (a) 500 m/s, (b) 1500 m/s, and (c) 2500 m/s

The resolidification starts from the center portion of the droplet when the droplet velocity is relatively low as shown in Fig. 4(a). On the contrary, the resolidification starts from the outside edge of the droplet when the droplet velocity is relatively high as shown in Fig. 4(c).

2.2 Influence of Droplet Diameter

The influence of the droplet diameter on the flattening behavior is discussed here for a droplet velocity of 2500 m/s. The horizontal traveling distance and the behavior of the atoms in the droplet and substrate are shown in Fig. 5 when $d = 3.1$ to 12.4 nm. It can be understood that the deformation in the horizontal direction becomes larger in proportion to the droplet diameter.

The atomic trajectories in representative positions in the droplet and the potential energy of each atom in the resolidification process are shown in Fig. 6 and 7 when $d = 6.3$ nm and $V_D = 2500$ m/s, respectively. From Fig. 6 and 7, it can be also understood that both the atomistic flow and the resolidification show similar trends as those shown in Fig. 3(c) and 4(c), respectively.

2.3 Influence of Impact Parameters

The effect of the impact parameters on the flattening ratio is discussed in this section. Figure 8 shows the relationship between the flattening ratio and the droplet velocity at various droplet diameters. The flattening ratio increases in proportion to the droplet velocity, and the gradient increases in proportion to the droplet diameter. It can be also understood that the flattening ratio when $d < 10$ nm does not approach 1 even when $V_D = 0$. This should be one of the unique characteristics in such a nanoscopic flattening process due to a nanoparticle.

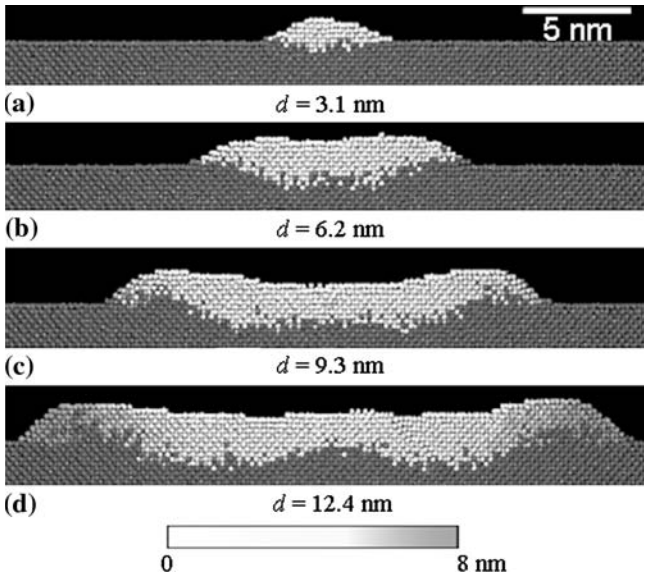

Fig. 5 Deformation process of droplet and traveling distance of atoms in horizontal direction ($VD = 2500$ m/s). d = (a) 3.1 nm, (b) 6.2 nm, (c) 9.3 nm, and (d) 12.4 nm

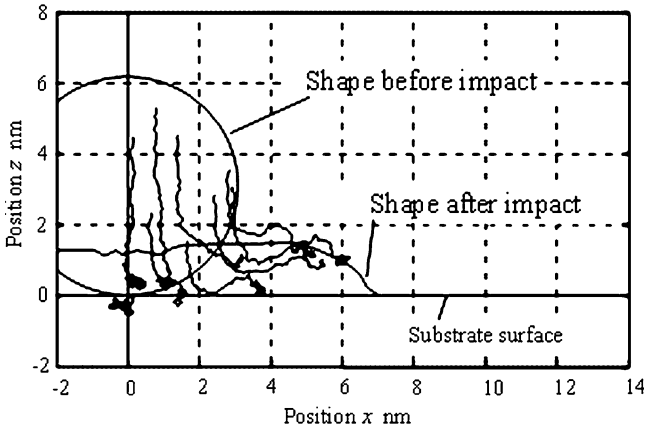

Fig. 6 Trajectory of some atoms in droplet ($VD = 2500$ m/s, $d = 6.2$ nm)

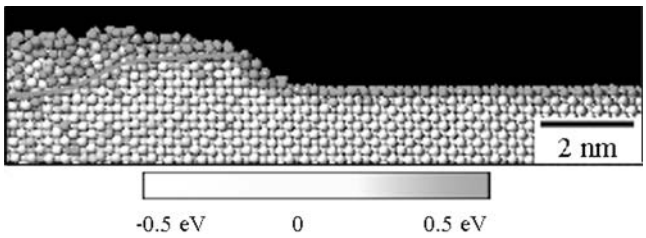

Fig. 7 Relationship between deformation and solidification process of droplet and potential energy of atoms ($VD = 2500$ m/s, $d = 6.2$ nm)

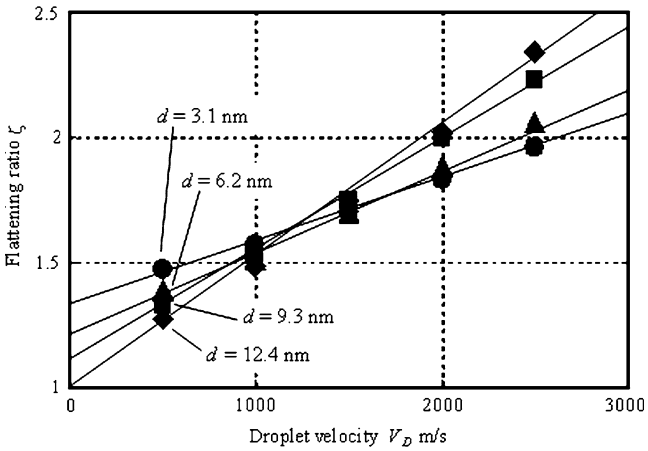

Fig. 8 Relationship between flattening ratio and droplet velocity at various droplet diameters

Figure 9 and 10 show the relationship between the flattening ratio and Reynold's number $\mathrm{Re} = \rho d V_D/\eta$ (ρ is specific mass; η is viscosity), and the Weber number $\mathrm{We} = \rho d V_D^2/\gamma$ (γ is surface tension), respectively, as used by Madejski (Ref 4). From these figures, it also turned out that the variation form of the flattening ratio is affected by the droplet diameters.

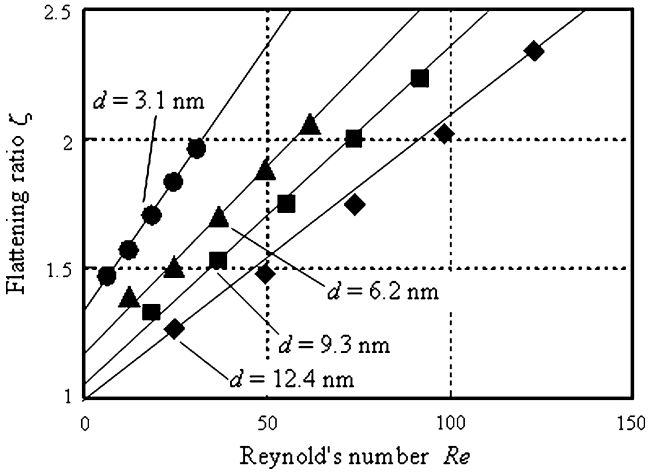

Fig. 9 Relationship between flattening ratio and Reynold's number at various droplet diameters

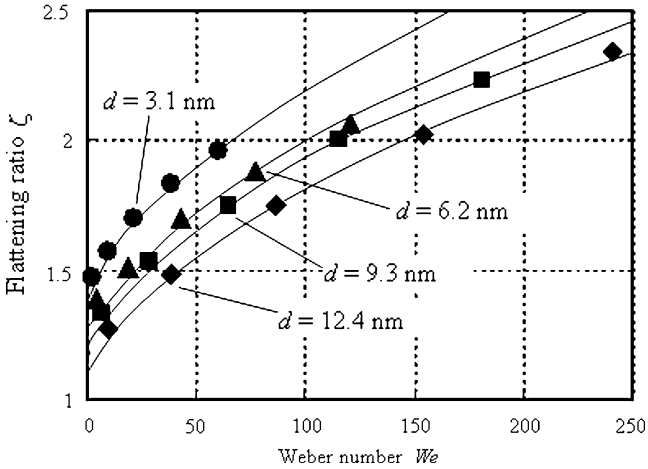

Fig. 10 Relationship between flattening ratio and Weber number at various droplet diameters

So, we assume that both the viscosity and the surface tension can be expressed as functions of the droplet diameter to consider the effect of nanoparticle (Ref 26) on such physical parameters, because these parameters should approach 0 when $d = 0$ and should also approach their macroscopic values when $d > 10$ nm. Figure 11 and 12 show the viscosity and the surface tension that were proposed here as functions of the droplet diameter. The functions proposed for the viscosity and surface tension of nanosized droplet are $\eta = 0.5602 \times 10^{-3}\{1 - \exp(-0.28\,d)\}$ Pa s and $\gamma = 0.7156\{1 - \exp(-0.28d)\}$ N/m, respectively.

Figure 13 and 14 show the improved data of the relationship between the flattening ratio and Reynold's number, and the Weber number, respectively, by using the parameters shown in Fig. 11 and 12. In Fig. 13, the flattening ratio increases in proportion to the Reynold's number with the same gradient independent from the droplet diameter. Especially, the flattening ratio shows

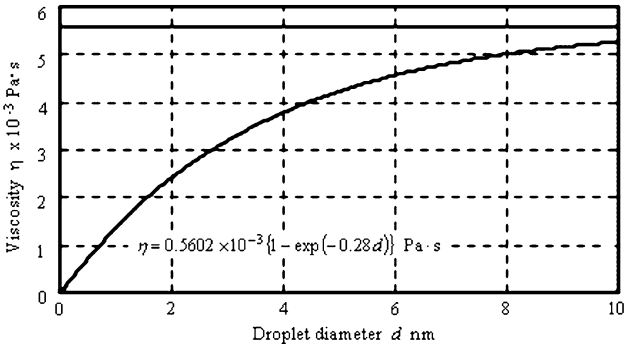

Fig. 11 Viscosity as a function of droplet diameter

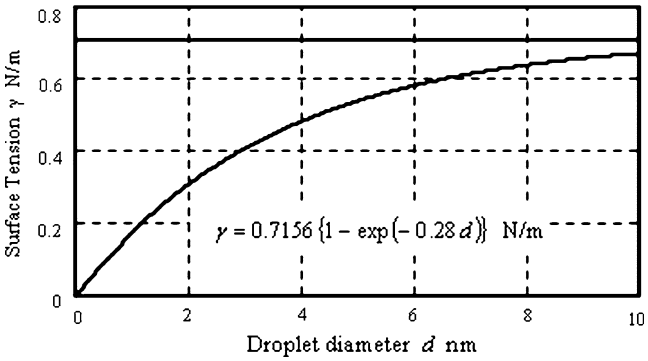

Fig. 12 Surface tension as a function of droplet diameter

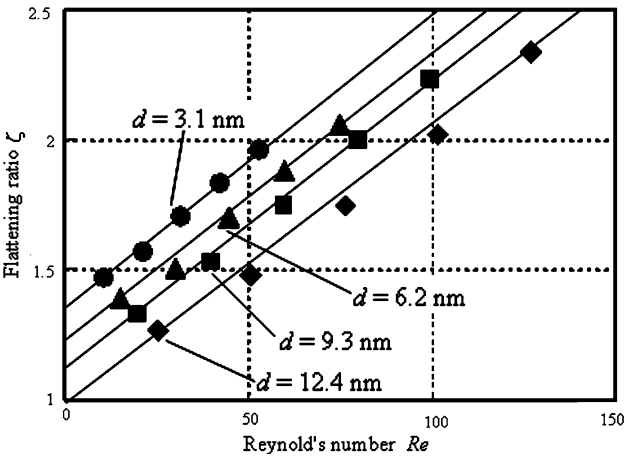

Fig. 13 Relationship between flattening ratio and Reynold's number, which is improved by viscosity in Fig. 11

$\xi = 0.012\ \mathrm{Re} + 1$ (correlation factor is 0.997) by a least squares calculation when $d = 12.4$ nm. In Fig. 14, the flattening ratio increases in proportion to the square root of the Weber number and the difference due to the droplet diameter becomes smaller with increase of the Weber number. Especially, the flattening ratio shows

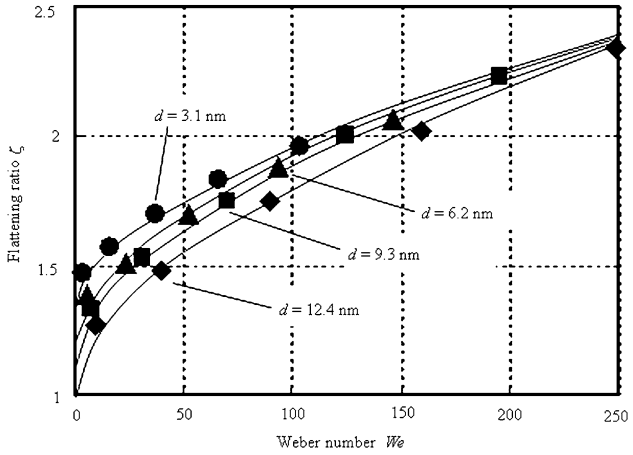

Fig. 14 Relationship between flattening ratio and Weber number, which is improved by surface tension in Fig. 12

$\xi = 0.078\ \mathrm{We}^{1/2} + 1$ (correlation factor is 0.989) by a least squares calculation when $d = 12.4$ nm.

These results show that the flattening ratio for nano-sized droplet can be reorganized by the same dimensionless parameters of the proper physical properties, such as the viscosity and the surface tension, as those used in the macroscopic flattening process (Ref 4). A comparison of the results with that of the references aforementioned (Ref 4-19) is difficult at this stage, because the target materials, the range of the velocity and size, and so on, are very different each other. So, this is an issue for the future.

3. Conclusions

Several three-dimensional molecular dynamics simulations were conducted to clarify at an atomic level the influences of the impact parameters, such as the droplet velocity and the droplet diameter, on the flattening behavior and the flattening ratio. In this study, we examined the impact on an Al substrate of an Al droplet with an initial temperature approximately 550 K higher than the melting point. In particular, the influences of impact velocity and droplet diameter on flattening behavior were evaluated. As a result, the following conclusions were obtained:

- The flattening ratio increases in proportion to the droplet velocity and the droplet diameter.
- The resolidification starts from the center portion of the droplet when the droplet velocity is relatively low. On the contrary, it starts from the outside edge of the droplet when the droplet velocity is relatively high.
- The flattening ratio when the droplet diameter is less than 10 nm does not approach 1 even when the droplet velocity approaches 0. This should be one of the unique characteristics in such a nanoscopic flattening process due to a nanoparticle.

- The flattening ratio for nanosized droplet can be reorganized by the same dimensionless parameters of the proper physical properties, such as the viscosity and the surface tension, as those used in the macroscopic flattening process.

Acknowledgments

This research was partially supported by the Takahashi Industrial and Economic Research Foundation, Japan.

References

1. L. Pawlowski, The Science and Engineering of Thermal Spray Coatings. John Wiley & Sons, Chichester, UK, 1995
2. D.B. Chrisey and G.K. Hubler, Pulsed Laser Deposition of Thin Films. John Wiley & Sons, Chichester, UK, 1994
3. V.I. Merkulov, D.H. Lowndes, G.E. Jellison, Jr., A.A. Puretzky, and D.B. Geohegan, Structure and Optical Properties of Amorphous Diamond Films Prepared by ArF Laser Ablation as a Function of Carbon Ion Kinetic Energy, *Appl. Phys. Lett.*, 1998, **73**(18), p 2591-2593
4. J. Madejski, Solidification of Droplets on a Cold Surface, *Int. J. Heat Mass Transfer*, 1976, **19**, p 1009-1013
5. J.P. Delplanque and R.H. Rangel, An Improved Model for Droplet Solidification on a Flat Surface, *J. Mater. Sci.*, 1997, **32**(6), p 1519-1530
6. M. Pasandideh-Fard, Y.M. Qiao, S. Chandra, and J. Mostaghimi, Capillary Effects During Droplet Impact on a Surface, *Phys. Fluids*, 1996, **8**(3), p 650-659
7. M. Pasandideh-Fard, R. Bhola, S. Chandra, and J. Mostaghimi, Deposition of Tin Droplets on a Steel Plate: Simulations and Experiments, *Int. J. Heat Mass Transfer*, 1998, **41**, p 2929-2945
8. H. Jones, Cooling, Freezing and Substrate Impact of Droplets Formed by Rotary Atomization, *J. Phys. D, Appl. Phys.*, 1971, **4**, p 1657-1660
9. G. Trapaga and J. Szekely, Mathematical Modeling of the Isothermal Impingement of Liquid Droplets in Spraying Processes, *Metall. Trans.*, 1991, **22B**, p 901-914
10. G. Trapaga and J. Szekely, Fluid Flow, Heat Transfer, and Solidification of Molten Metal Droplets Impinging on Substrates: Comparison of Numerical and Experimental Results, *Metall. Trans.*, 1992, **23B**, p 701-718
11. E. Nishioka and M. Fukumoto, Flattening Behavior of Freely Fallen Molten Metal Droplet on Flat Substrate, *Quart. J. Jpn. Weld. Soc.*, 1998, **16**(4), p 437-444
12. M. Fukumoto, H. Nagai, and T. Yasui, Influence of Surface Character Change of Substrate Due to Heating on Flattening Behavior of Thermal Sprayed Particles, *J. Therm. Spray Technol.*, 2006, **15**(4), p 759-764
13. L. Li, A. Vaidya, S. Sampath, H. Xiong, and L. Zheng, Particle Characterization and Splat Formation of Plasma Sprayed Zirconia, *J. Thermal Spray Technol.*, 2006, **15**(1), p 97-105
14. P. Fauchais, M. Fukumoto, A. Vardelle, and M. Vardelle, Knowledge Concerning Splat Formation: An Invited Review, *J. Thermal Spray Technol.*, 2004, **13**(3), p 337-360
15. P. Gougeon and C. Moreau, Simultaneous Independent Measurement of Splat Diameter and Cooling Time During Impact on a Substrate of Plasma Sprayed Molybdenum Particles, *J. Thermal Spray Technol.*, 2001, **10**(1), p 76-82
16. A. McDonald, M. Lamontagne, S. Chandra, and C. Moreau, Photographing Impact of Plasma-Sprayed Particles on Metal Substrates, *J. Thermal Spray Technol.*, 2006, **15**(4), p 708-716
17. M. Xue, S. Chandra, and J. Mostaghimi, Investigation of Splat Curling up in Thermal Spray Coatings, *J. Thermal Spray Technol.*, 2006, **15**(4), p 531-536
18. N.Z. Mehdizadeh, M. Lamontagne, C. Moreau, S. Chandra, and J. Mostaghimi, Photographing Impact of Molten Molybdenum Particles in a Plasma Spray, *J. Thermal Spray Technol.*, 2005, **14**(3), p 354-361
19. Y. Shibuta and S. Maruyama, Molecular Dynamics Simulation of Formation Process of Single-walled Carbon Nanotubes by CCVD Method, *Chem. Phys. Lett.*, 2003, **382**(3-4), p 381-386
20. K. Tanaka, T. Kato, and Y. Matsumoto, Molecular Dynamics Simulation of Vibrational Friction Force Due to Molecular Deformation in Confined Lubricant Film, *ASME J. Tribol*, 2003, **125**(3), p 587-591
21. T. Inamura, S. Shimada, N. Takezawa, and N. Nakahara, Brittle/Ductile Transition Phenomena Observed in Computer Simulations of Machining Defect-Free Monocrystalline Silicon, *Ann. CIRP*, 1997, **46**(1), p 31-34
22. J. Shimizu, E. Ohmura, Y. Kobayashi, S. Kiyoshima, and H. Eda, Molecular Dynamics Analysis of Elementary Process of Coating by a High-Temperature, High-Speed Droplet (Flattening Process and Atomic Behavior of a Droplet), *JSME (Jpn. Soc. Mech. Eng.) Int. J. Series C*, 2006, **49**(2), p 505-511
23. R.W. Hockney, The Potential Calculation and Some Applications, *Meth. Comput. Phys.*, 1969, **9**, p 135
24. L.A. Girifalco and V.G. Weizer, Application of the Morse Potential Function to Cubic Metals, *Phys. Rev.*, 1959, **114**, p 687-690
25. J. Shimizu, E. Ohmura, and H. Eda, Analysis of Sliding Mechanism Using Molecular Dynamics: Friction Process, *Jpn. J. Trib.*, 1996, **41**(12), p 1375-1386
26. J. Farges, M.F. de Feraudy, B. Raout, and G. Torchet, Noncrystalline Structure of Argon Clusters, *J. Chem. Phys.*, 1986, **84**(6), p 3491-3501